Research Article

Samar Moustafa, Atif Mossad Ali, Jawaher Shawaf, Sharah H. Al dirham, Norah Alqhtani, Salah A. Al-Ghamdi, Saloua Helali, Hesham Fares, and Mohamed Rashad*

Linear and nonlinear optical studies on successfully mixed vanadium oxide and zinc oxide nanoparticles synthesized by sol–gel technique

https://doi.org/10.1515/ntrev-2024-0041
received December 23, 2023; accepted May 17, 2024

Abstract: In this study, V_2O_5, $5ZnO/10V_2O_5$, and ZnO, $10ZnO/10V_2O_5$ nanocomposites were synthesized by the sol–gel method. The sol–gel technique is an important process for the fabrication of advanced oxide materials with desirable catalytic, optical, and structural properties. The varieties and flexibilities of sol–gel techniques help in preparing materials with extremely specific properties. For the presented samples, three types of phases were assessed. The average crystalline size of V_2O_5, $5ZnO/10V_2O_5$ and ZnO, $10ZnO/10V_2O_5$ nanocomposites were found to be 25, 26, 14.5, and 15.5 nm, respectively. SEM images showed three different shapes of semi-tube, semi-spherical, and semi-flower. The pure samples of V_2O_5 and ZnO showed semi-tube shapes. $5ZnO/10V_2O_5$ shows a spherical shape with average dimeter of 0.6 µm. Strong dependence of the direct optical band gap was observed on different compositions that varied within the range of (2.33–2.73 eV). Conversely, the indirect values varied within the range of 2.119–2.35 eV. On the other hand, $10ZnO/10V_2O_5$ has semi flower shape with different layers. Optical parameters, such as optical band gap, extension coefficient, tails of localized states, and refractive index, were gauged for these nanocomposites. In addition, the mean refractive index of ZnO is lower than that of V_2O_5, with differences observed between $5ZnO/10V_2O_5$ and $10ZnO/10V_2O_5$ nanocomposites.

Keywords: mixed oxides, ZnO, V_2O_5, optical band gap, nonlinear optical studies

*** Corresponding author: Mohamed Rashad,** Department of Physics, Faculty of Science, University of Tabuk, Tabuk, Saudi Arabia, e-mail: m.ahmad@ut.edu.sa
Samar Moustafa: Physics Department, Faculty of Science, Taibah University, P. O. Box 30002, Medina, Saudi Arabia; Physics Department, Faculty of Science, Assiut University, Assiut, 71516, Egypt
Atif Mossad Ali, Jawaher Shawaf, Sharah H. Al dirham, Norah Alqhtani: Physics Department, Faculty of Science, King Khalid University, Abha, Saudi Arabia
Salah A. Al-Ghamdi, Saloua Helali: Department of Physics, Faculty of Science, University of Tabuk, Tabuk, Saudi Arabia
Hesham Fares: Physics Department, Faculty of Science, Taibah University, P. O. Box 30002, Medina, Saudi Arabia

1 Introduction

Nanocrystalline metal oxides with uniform shapes and sizes are considered one of the main building blocks of nanotechnology owing to their high surface area, surface chemistry, and intrinsic optical and catalytic characteristics [1,2]. In addition, these metal oxides offer advantageous electronic and optical properties by combining different properties of their constituent materials. The electronic structures, charge transportation characteristics, and light absorption properties are the key aspects of metal oxides that determine their prowess as photocatalysts. A photocatalyst is a material that can absorb light and produce electron/hole pairs (e^-/h^+), thus enabling chemical transformations of reactants and regenerating its chemical composition after each cycle of such interactions. The main features of a photocatalytic system are wide optical band gap energy (E_g), suitable morphology, high surface area, excellent stability, and reusability.

Recently, photocatalysts garnered a lot of attention from scientists because of their appealing applications toward the advantage of humanity. Among these, vanadium-based oxides, especially vanadium pentoxide (V_2O_5), are broadly considered due to their exceptional properties [3]. Due to its promising and remarkable optoelectronic properties [4], gas sensors, storage systems, laser scanners, thermochromic coatings, solar cells, optical fiber switching devices, batteries, IR detectors, and ultrafast switching applications [5–13] are applicable to V_2O_5. ZnO is an n-type semiconductor material with a wide E_g of 3.37 eV at 300 K and a large exciton binding energy of about 60 meV. Research is currently being conducted to investigate its potential use in optoelectronics, sensors, and ferroelectric memory devices [14].

One of the unique inorganic semiconductor materials is metal-doped zinc oxide (Ni, Co). Based on the oxygen vacancies and wurtzite structure, it has a large exciton binding energy of 60 meV at room temperature and a wide direct bandgap of 3.37 eV [15]. Because of its use in optoelectronic devices, ZnO is a significant II–IV n-type direct bandgap semiconductor material that has garnered a lot of attention [16]. It is regarded as a multifunctional semiconductor compound because of its good physical properties [17]. ZnO belongs to the II–VI groups of the periodic table and manifests three crystalline structures: wurtzite, rock salt (NaCl or Rochelle salt), and zinc blend (ZnS). The wurtzite form is the thermodynamically stable phase under ambient conditions. The wurtzite ZnO exhibits intriguing optical, electrical, and optoelectronic properties in both thin-film and nanostructured forms [18]. The properties of ZnO mainly depend on the growth parameters, such as temperature, concentrations of solutions, the stoichiometry of reagents, and pH of the synthesis method [19]. The size, orientation, density, and morphology of ZnO crystal mainly contribute to numerous applications. The physical properties of ZnO are mainly affected by dopant impurities and defects [18]. Defects play an important role in obtaining desirable optoelectronic and electronic properties of semiconductor materials. ZnO can be fabricated in several shapes, such as single crystal, pellet, fine powder, and thick and thin films. Different experimental conditions, such as solution concentration, temperature, and substrate pretreatment, greatly influence the growth and shape of ZnO nanostructure; therefore, a good understanding of the ZnO growth condition is imperative. The applications of ZnO can be found in electronic apparatuses [20], for eco-friendly buffer layer for thin film solar cell applications [21], gas sensors [17], and photocatalysis processes [22]; hence, modifications of its properties are essential for both practical and scientific interests.

Many nanostructured materials have been used as lithium-ion batteries electrode materials in the last 10 years due to significant advancements in materials science and nanotechnology. Because of its low cost, abundance, ease of synthesis, and good safety, layered V_2O_5 is one of the most appealing potential cathode materials and has been thoroughly studied [23]. Moreover, the cathode material, a crucial component of lithium-ion batteries, has a direct impact on how well these batteries function. However, there is still a need to further improve the energy and power density of electrode materials due to the growing demand for high-power and high-energy devices. V_2O_5 is thought to be the most promising metal oxide to use as a cathode material for lithium-ion batteries [24]. The kinetic behaviors of photogenerated carriers, which increase light absorption and significantly boost photocatalytic activity, are influenced by the heterostructures of V_2O_5. Determining the remaining optical and electrical properties of these materials requires an understanding of their structural and topographical characteristics as well as an understanding of the mechanism underlying grain growth [25,26]. Therefore, in this research, we will focus on these electrical and optical properties of ZnO–V_2O_5 nanocomposites. Therefore, the main purpose of this work is to investigate the structural and optical properties of ZnO–V_2O_5 nanocomposites.

2 Experimental technique

2.1 Materials

The chemicals used to prepare ZnO–V_2O_5 nanoparticles were distilled water, zinc acetate $Zn(CH_3COO)_2(H_2O)_2$, and ammonium metavanadate (NH_4VO_3). Four samples (pure ZnO, pure V_2O_5, 0.5% ZnO-1.0%V_2O_5, and 1.0%ZnO-1.0%V_2O_5 (molar ratio)) were prepared by the sol–gel method.

2.2 Methods

To synthesize ZnO/V_2O_5 nanocomposites, various routes were proposed, such as the solvothermal process, homogeneous co-precipitation method [27], pulsed-laser ablation [28], electrospinning method [24], spray pyrolysis technique [29], and the sol–gel method [30]. The sol–gel method was used to synthesize metal oxide nanocomposite specimens. The narrow particle size distribution, uniform nanostructure at low temperatures, and high product purity are the main benefits of the sol–gel process. Metal nanooxides are frequently synthesized using this technique [31]. High-purity metal salt powders were used to prepare ZnO–V_2O_5 nanocomposite specimens. In the experiment, (NH_4VO_3) was added to 100 mL of distilled water, and the solution was stirred using a magnetic stir bar at 55°C for 30 min ($(CH_3.COO)_2Zn{\cdot}2H_2O$) was added to the above solution. The stirring of the solution was continued for additional 2 h. The obtained mixture was stirred at room temperature for 24 h

Scheme 1: The steps of the used chemical method.

utilizing a magnetic stirring hotplate to produce a homogenous solution. Scheme 1 shows the steps of the used chemical method.

Upon the completion of the stirring, the mixture was dried at 120°C for 24 h. The solution was then gradually dried until it became an amorphous solid or a gel. The as-prepared samples were annealed at 500°C for 3 h. The gel was annealed at high temperatures to crystallize the amorphous solid and to remove the residual carbon and organic chemicals. The properties of ZnO/V_2O_5 were measured to achieve the desired doping concentration.

2.3 Characterizations

Using X-ray Diffraction (XRD) of Cu-Kα radiation of 1.5406 Å, the structural investigation of ZnO–V_2O_5 nanocomposites was done. Moreover, the optical properties were assessed using an Ultraviolet-Visible (UV-vis) spectroscopy. SEM (JEOL Type T200) was used to examine the morphology of samples at 15 kV. Using ImageJ software, a few hundred of the particles were measured in order to estimate the particle size distribution. Reflectance (R) was in the range of wavelength 190–1,000 nm, gauged using a Shimadzu UV-2101 spectrophotometer.

3 Results and discussion

3.1 Structural investigations

XRD spectra were analyzed for the crystal structures. Figure 1 shows the XRD charts of V_2O_5, 5ZnO/10V_2O_5 and ZnO, 10ZnO/10V_2O_5 nanocomposites. Three types of phases are detected and illustrated in Figure 1. The first phase type indexed well to orthorhombic-structured V_2O_5 (JCPDS card no: 41-1426). The main reflection peaks at 2θ values, 15.6°, 20.3°, 21.7°, 26.3°, 31.17°, 32.4°, 34.47°, 41.39°, 45.6° and 47.5°, were attributed to the (200), (001), (101), (110), (400), (011), (310), (002), (411) and (600) crystal planes, respectively, of the V_2O_5. On the other hand, the second phase found was a hexagonal ZnO structure (JCPDS card no: 36-1451).

The peaks at 2θ were 31.86°, 34.5°, 36.27°, 47.59, 56.7, 63.0, 66.46, 58.1, 69.2, 72.5 and 77.1 which were attributed, respectively, to the (100), (002), (101), (102), (110), (103), (200), (112), (201), (004) and (202) of ZnO nanoparticles. These peaks positions error is ±0.2. The most important phase was ZnV_2O_6. The obtained ZnV_2O_6 nanostructures exhibited promising hydrogen absorption.

The average crystallite size (D) using Scherrer's equation, dislocation density (δ), and microstrain (ε) for the V_2O_5, 5ZnO/10V_2O_5 and ZnO, 10ZnO/10V_2O_5 nanocomposites has been calculated as [32–34]: $D = \frac{K\lambda}{\beta\cos(\theta)}$ and $\delta = \frac{1}{D^2}$, *w*here the constant K is a function of the crystallite shape which is generally taken as being about unity, and β is the full width at half of the maximum intensity of the diffracted peaks. The average calculated values of D for the V_2O_5, 5ZnO/10V_2O_5 and ZnO, 10ZnO/10V_2O_5 nanocomposites were found to be 25, 26, 14.5, and 15.5 nm, respectively. Table 1 shows the recorded values of examined crystal structure parameters, such as D, δ, and ε, for all samples. The values of δ and ε exhibit opposite behaviors compared to the value of D.

The surface morphology of the V_2O_5, 5ZnO/10V_2O_5 and ZnO, 10ZnO/10V_2O_5 nanocomposites is illustrated in Figure 2 in two different magnifications. The image of the V_2O_5 shows a semi tube shape with length and width of 1.12 and 0.2 µm, respectively. On the other hand, 5ZnO/10V_2O_5 nanocomposite shows a spherical shape with average dimeter of 0.6 µm. Regarding the ZnO nanocomposite, it shows again semi-tube

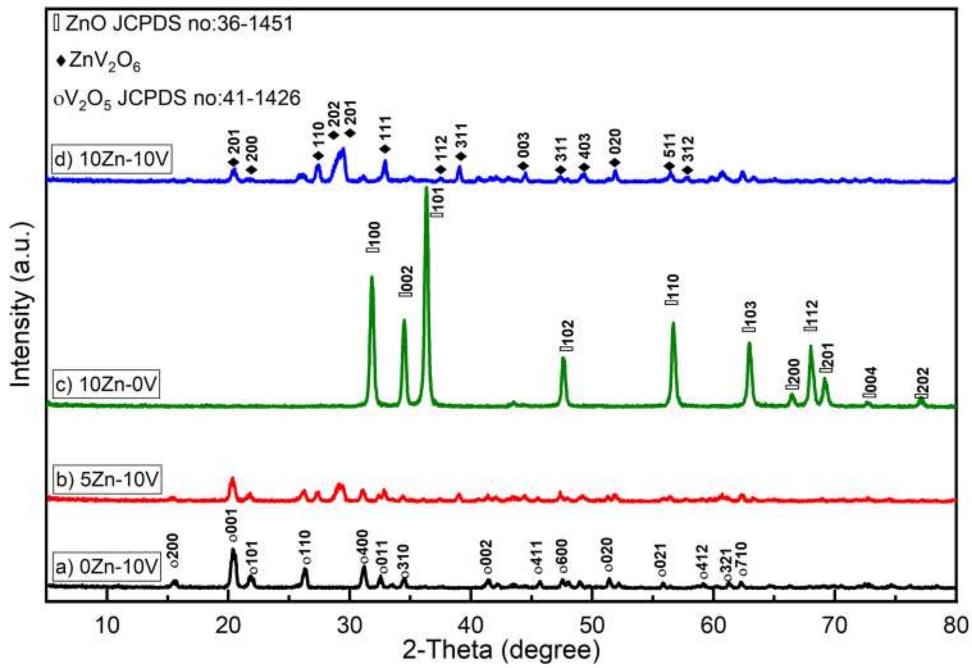

Figure 1: XRD charts of (a) V_2O_5, (b) $5ZnO/10V_2O_5$, (c) ZnO, and (d) $10ZnO/10V_2O_5$ nanocomposites.

Table 1: Structural parameters for V_2O_5, $5ZnO/10V_2O_5$, ZnO, 10ZnO/ $10V_2O_5$ nanocomposites

Nanocomposites	*D* (nm)	δ (nm^{-2}) × 10^{-3}
$0ZnO/10V_2O_5$	25	1.6
$5ZnO/10V_2O_5$	26	1.5
$10ZnO/0V_2O_5$	14.5	4.7
$10ZnO/10V_2O_5$	15.5	4.2

shape with length and width of 0.44 and 0.12 µm, respectively. Finally, $10ZnO/10V_2O_5$ nanocomposite shows a semi flower shape with different layers with length and width of 1 µm. By measuring several hundred particles from the SEM image, the particle size distribution was computed using ImageJ software. The average size of $5ZnO/10V_2O_5$ is found to be smaller than that of V_2O_5. The nucleation process may be responsible for the phenomenon's potential. A faster rate of nucleation leads to a higher concentration of nanoparticles. It is interesting to note that semi-flower $10ZnO/10V_2O_5$ has a smaller average size than ZnO. This indicates that the presence of V_2O_5 particles within the nanocomposite can inhibit particle growth, leading to a reduction in size [35].

To confirm the presence, composition, and homogeneity of all elements in the samples, we have performed the EDX analyses as displayed in Figure 3. Figure 3(a) indicates the presence of V and O in pure V_2O_5, while Figure 3(b) shows the presence of Zn and O in ZnO, and Figure 3(c) and (d) shows the presence of V, Zn, and O in the final composites.

3.2 Linear optical investigations

3.2.1 Optical absorption region

The optical properties of V_2O_5, $5ZnO/10V_2O_5$ and ZnO, $10ZnO/10V_2O_5$ nanocomposites were probed by room-temperature UV-Vis Diffusion Reflectance Spectra (UV-Vis DRS). The diffusion reflectance (*R*%) spectra of V_2O_5, 5ZnO/ $10V_2O_5$, and ZnO, $10ZnO/10V_2O_5$ nanocomposites are shown in Figure 4. It is observed that the prepared ZnO/V_2O_5 gives a strong visible absorption edge at spectra at around 410 nm. UV-vis measurements were executed in diffusion reflectance mode (*R*) and converted to the Kubelka-Munk function *F*(*R*) to separate the light absorption from scattering. The absorption coefficient $\alpha = (R)$ was found utilizing the Schuster–Kubelka–Munk function expressed as follows [36]:

$$\alpha(R) = \frac{(1-R)^2}{2R}, \tag{1}$$

where *R* represents the diffusion reflectance.

The absorption coefficient *vs* photon energy for V_2O_5, $5ZnO/10V_2O_5$ and ZnO, $10ZnO/10V_2O_5$ nanocomposites are shown in Figure 5. At $E \geq 3.1$ eV, the α is higher vaue, on the constract, the minimum value of α at green area. Moreover, it was noticed that at the lower region of absorption, α value as a function of photon energy obeyed the Urbach relation [37].

$$\alpha(\upsilon) = \alpha_0 \exp(h\upsilon/E_r), \tag{2}$$

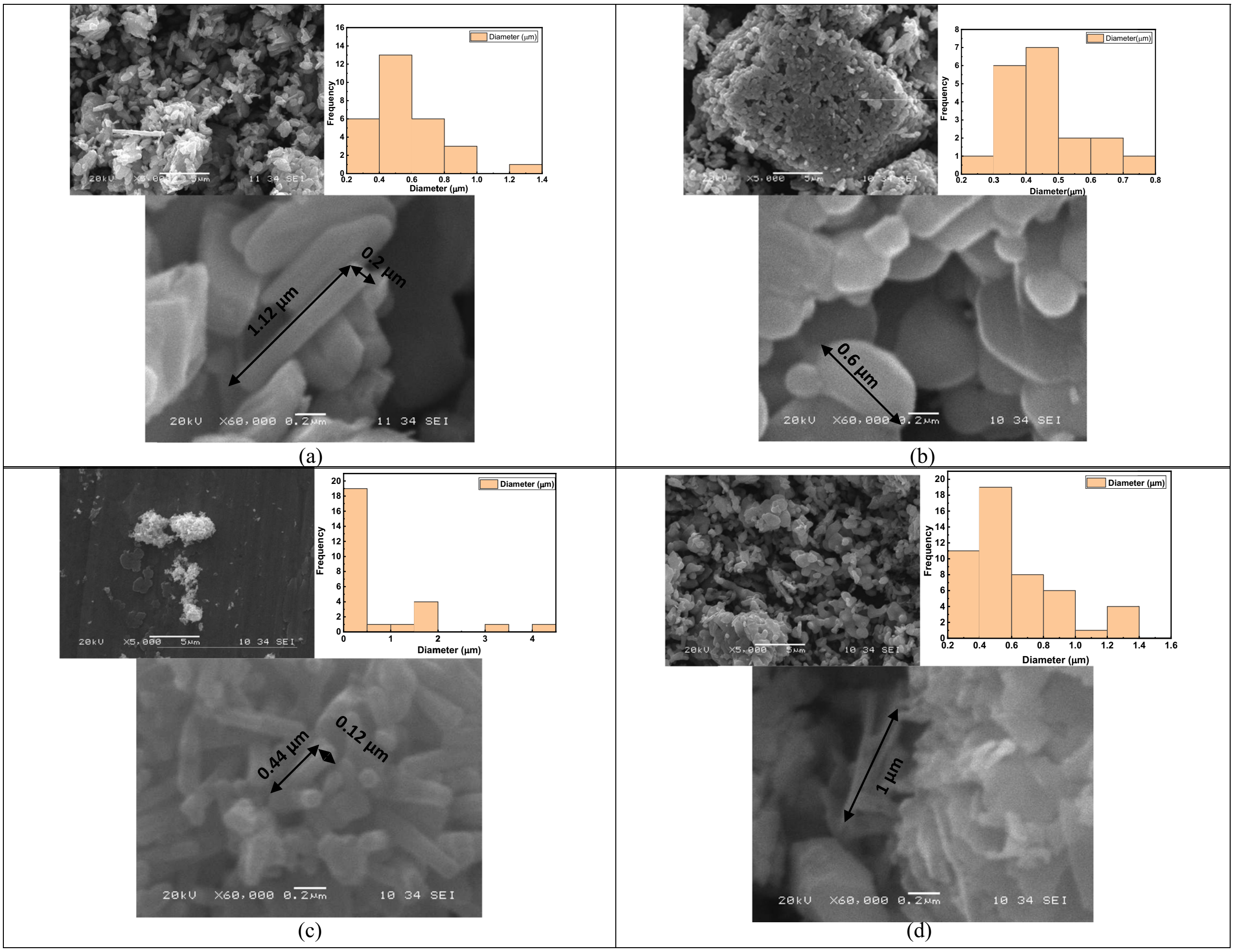

Figure 2: SEM images of (a) V_2O_5, (b) $5ZnO/10V_2O_5$, (c) ZnO, and (d) $10ZnO/10V_2O_5$ nanocomposites. Insert Figure: another magnifications of the images, nanocomposites size distribution determined with ImageJ software.

where α_o is a constant, and the Urbach tail width is represented by E_r.

A relation between $\ln(\alpha)$ and $h\upsilon$ for the V_2O_5, $5ZnO/10V_2O_5$ and ZnO, $10ZnO/10V_2O_5$ nanocomposites is presented in Figure 6. The evaluated E_r for various samples is computed from the slope in Figure 6 and is listed in Table 2. The change in E_r corresponding to the change in ZnO/V_2O_5 ratio could be related to the change in the disorder degree which changes the band tailing.

The extinction coefficient ($k_{ext.}$) for the V_2O_5, $5ZnO/10V_2O_5$ and ZnO, $10ZnO/10V_2O_5$ nanocomposites is investigated. Hence, $k_{ext.}$ can be computed from [37]:

$$k_{ext.} = \frac{\alpha\lambda}{4\pi}. \tag{3}$$

The plots of k_{ext} *vs* λ of the incident electromagnetic waves for V_2O_5, $5ZnO/10V_2O_5$ and ZnO, $10ZnO/10V_2O_5$ nanocomposites are illustrated in Figure 7. It can be seen, $k_{ext.}$, of the V_2O_5, $5ZnO/10V_2O_5$ and ZnO, $10ZnO/10V_2O_5$ nanocomposites is steadily independent at λ for $\lambda > 550$ nm, while it significantly increased to peak values at $\lambda < 550$ nm. Besides, the value and peak position of $k_{ext.}$ are affected by the change in concentration of V_2O_5, $5ZnO/10V_2O_5$ and ZnO, $10ZnO/10V_2O_5$ nanocomposites. These peaks are attributed to the process of particle absorption.

The direct/indirect optical band gaps, E_g^{di} and E_g^{ind}, and absorption coefficient α are correlated through the equation [38]:

$$\alpha h\nu = B_1(h\nu - E_g^{di})^{\frac{1}{2}}, \tag{4}$$

where α represents linear absorption coefficient, $h\nu$ is the photon energy, and B_1 is the proportionality constant.

Using equation (1), we can compute the following expression [39]:

$$\alpha h\nu = B_2(h\nu - E_g^{ind})^2. \tag{5}$$

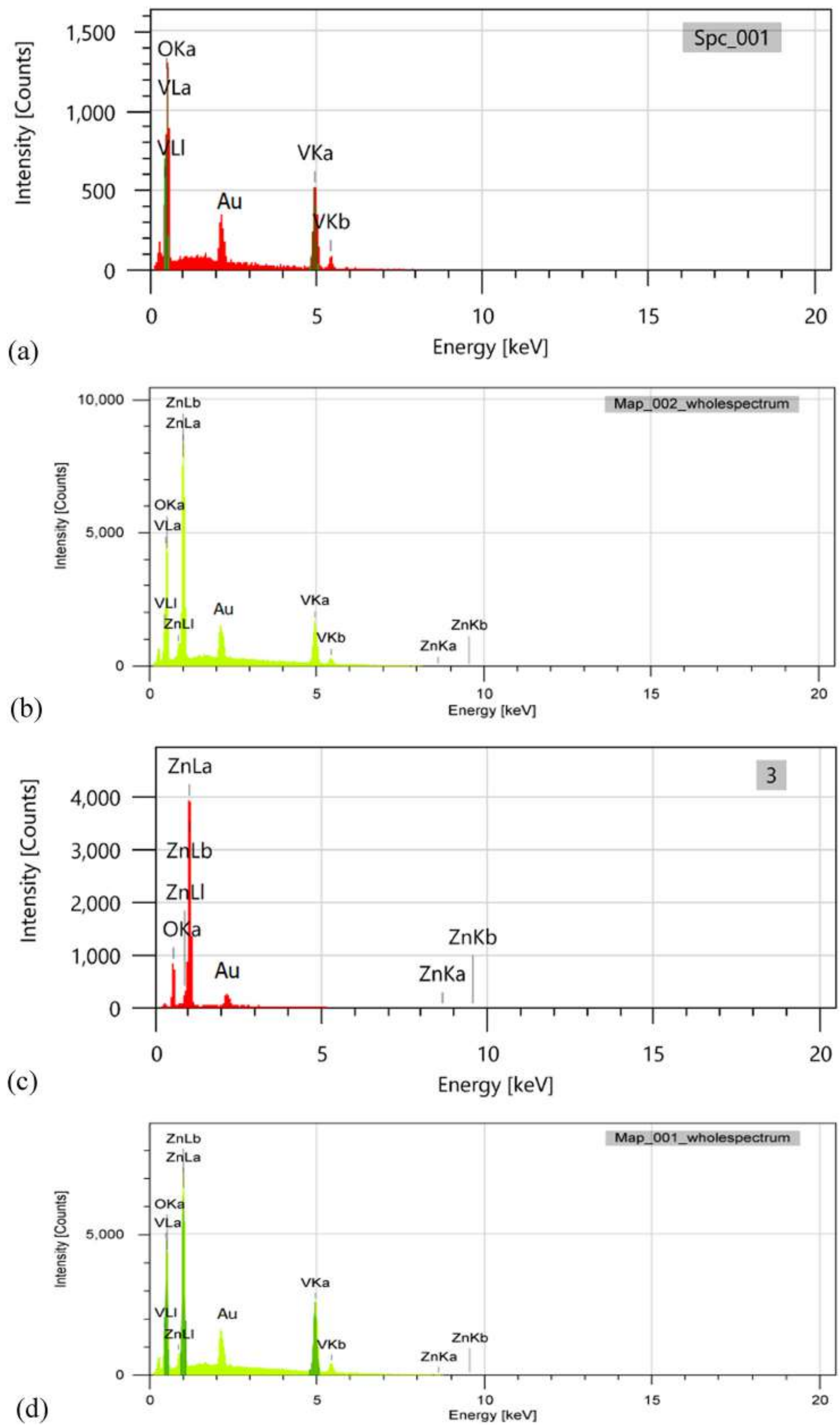

Figure 3: EDX of (a) V_2O_5, (b) $5ZnO/10V_2O_5$, (c) ZnO, and (d) $10ZnO/10V_2O_5$ nanocomposites (Au peak comes from sputtering system).

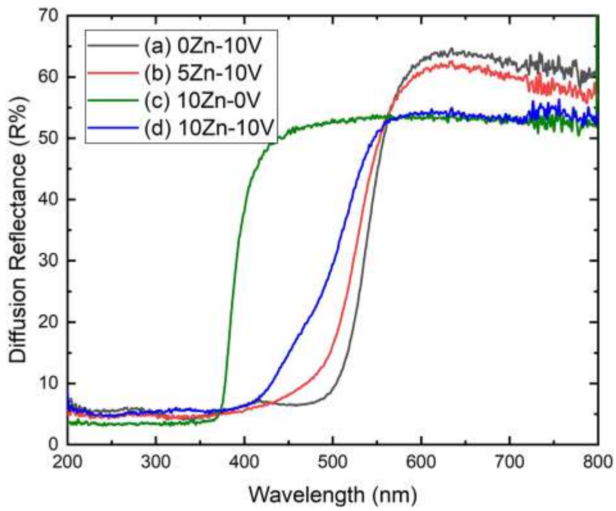

Figure 4: Reflectance charts of (a) V_2O_5, (b) $5ZnO/10V_2O_5$, (c) ZnO, and (d) $10ZnO/10V_2O_5$ nanocomposites.

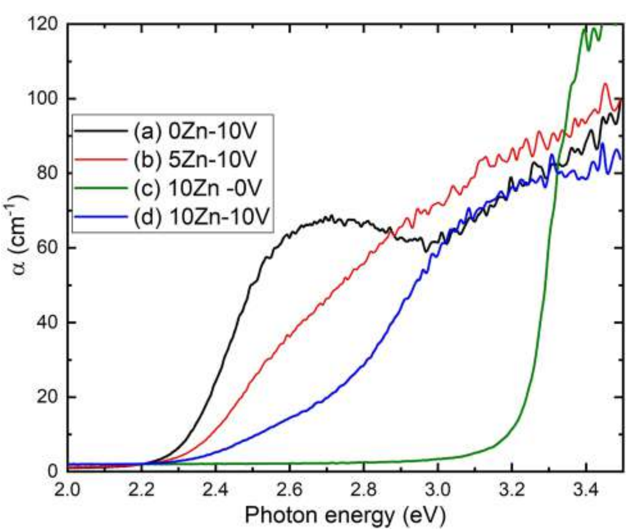

Figure 5: Absorption coefficient *vs* photon energy of (a) V_2O_5, (b) 5ZnO/$10V_2O_5$, (c) ZnO, and (d) $10ZnO/10V_2O_5$ nanocomposites.

Figures 8 and 9 show $(\alpha h\nu)^2$ and $(\alpha h\nu)^{1/2}$ against $h\nu$, respectively. The values of E_g^{di} and E_g^{ind} were calculated. These calculated values of both direct and indirect optical band gaps are tabulated in Table 2, which shows an opposite behavior to the value of E_r. The direct and indirect optical band gap of ZnO are 3.2 and 3.16 eV, respectively. These values are comparable with the reported values of ZnO (~3.1, 3.2, and 3.3 eV) [40], 3.63 eV [41], (3.17–3.24) eV [42]. On the other hand, direct and indirect optical band gap of V_2O_5 are 2.33 and 2.19 eV. The vanadium ions in the metallic phase (corundum) occupy two-thirds of the octahedral sites formed by oxygen anions [43]. These values of optical band gaps are compatible with pervious

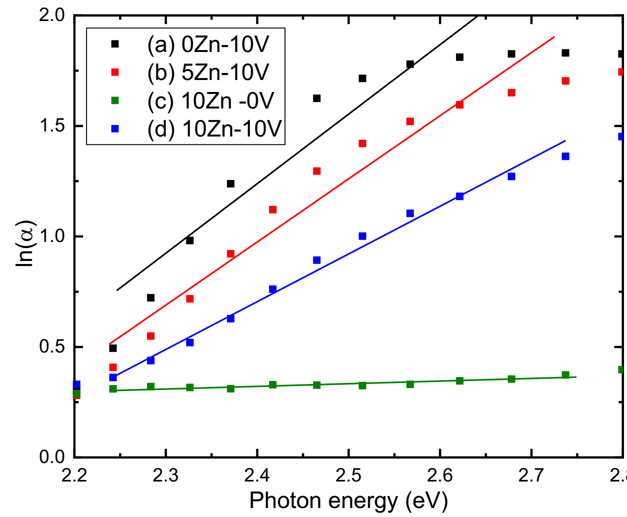

Figure 6: ln(α) *vs* photon energy of (a) V_2O_5, (b) $5ZnO/10V_2O_5$, (c) ZnO, and (d) $10ZnO/10V_2O_5$ nanocomposites.

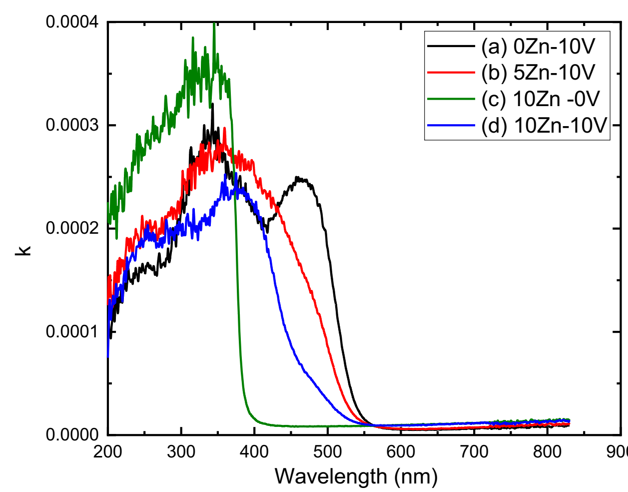

Figure 7: Extinction coefficient *vs* photon energy of (a) V_2O_5, (b) 5ZnO/$10V_2O_5$, (c) ZnO, and (d) $10ZnO/10V_2O_5$ nanocomposites.

reported values of 2.3 eV [44], 2.363 eV, and [45] 2.23 eV [46]. According to both literature review [14] and fitting factor (R^2) The majority types of transition in this samples is direct transition.

3.2.2 Relation between the refractive index and the energy gap

The values of static refractive index, n_o, can be calculated from the E_g^{dir} values. Few empirical equations showed the relation between n and E_g^{dir} that have been proposed by several models, but, there are some main models for calculating the refractive index using the optical band gap

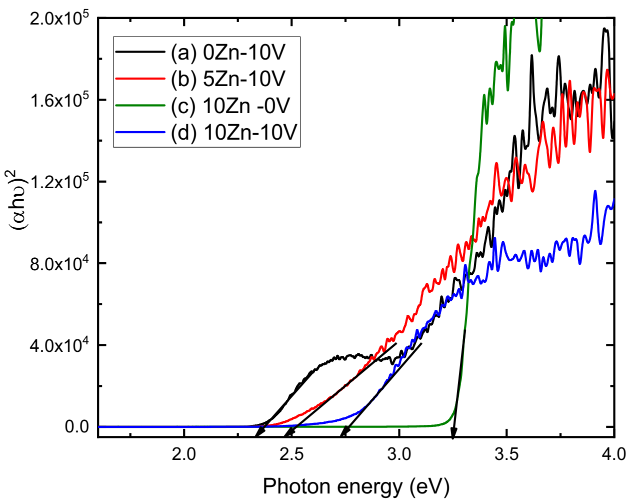

Figure 8: $(ah\nu)^2$ *vs* photon energy of (a) V_2O_5, (b) $5ZnO/10V_2O_5$, (c) ZnO, and (d) $10ZnO/10V_2O_5$ nanocomposites.

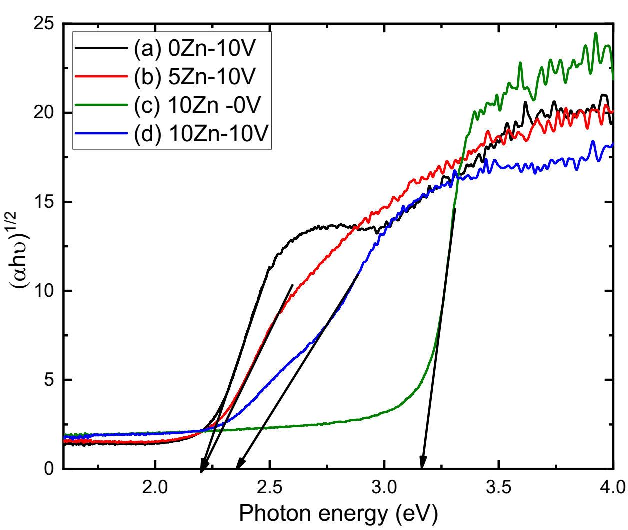

Figure 9: $(ah\nu)^{1/2}$ *vs* photon energy of (a) V_2O_5, (b) $5ZnO/10V_2O_5$, (c) ZnO, and (d) $10ZnO/10V_2O_5$ nanocomposites.

which called Moss, Ravindra, Reddy and Kumar and Singh models [47–54]. These values for V_2O_5, $5ZnO/10V_2O_5$ and ZnO, $10ZnO/10V_2O_5$ nanocomposites are listed in Table 3 using the different above models.

Table 2: Optical constants for V_2O_5, $5ZnO/10V_2O_5$, ZnO, $10ZnO/10V_2O_5$ nanocomposites

Nanocomposites	E_r (eV)	E_g^{di}(eV)	E_g^{ind}(eV)
$0ZnO/10V_2O_5$	0.32	2.33	2.19
$5ZnO/10V_2O_5$	0.35	2.46	2.20
$10ZnO/0V_2O_5$	0.47	3.20	3.16
$10ZnO/10V_2O_5$	8.33	2.73	2.35

Moss Model corrected by Ravindra [50]

$$n_{Rs} = \sqrt[4]{\frac{108}{E_g^d}}, \tag{6}$$

Ravindra and Guptau Model [50]

$$n_R = 4.084 - (0.62E_g), \tag{7}$$

Reddy and Anjanyuku Model [50,51]

$$n_{RA} = 3.59182 - \ln(E_g), \tag{8}$$

Kumar and Singh Model [48,53]

$$n_{KS} = 3.3668E_g^{-0.32234}. \tag{9}$$

The Z-scan technique was used for obtaining the value of the nonlinear refractive index and nonlinear absorption directly. Also, these values of the nonlinear refractive index could be determined from the calculated linear refractive index values which were recorded from reflectance and transmittance. Finally, it is found that the direct and indirect optical band gap of V_2O_5 is smaller than that of ZnO. On the other hand, the optical band gap of V_2O_5 increases for $5ZnO/10V_2O_5$ and $10ZnO/10V_2O_5$ nanocomposites.

3.3 Nonlinear optical investigations

The calculated values of the refractive index can be used to obtain other optical parameters, including the dielectric constant (ϵ_o), the third-order susceptibility ($\chi^{(3)}$), and nonlinear refractive index (n_2) from equations (10)–(12), respectively [23,55–57].

Table 3: Refractive index obtained from the deduced value of E_g by various approaches along with its average value for V_2O_5, $5ZnO/10V_2O_5$, ZnO, $10ZnO/10V_2O_5$ nanocomposites

Nanocomposites	E_g^{di}(eV)	n_{RS}	n_R	n_{RA}	n_{Ks}	$\bar{n}_{av.}$
$0ZnO/10V_2O_5$	2.33	2.61	2.64	2.75	2.56	2.64
$5ZnO/10V_2O_5$	2.46	2.57	2.56	2.69	2.52	2.59
$10ZnO/0V_2O_5$	3.20	2.41	2.1	2.43	2.31	2.31
$10ZnO/10V_2O_5$	2.73	2.51	2.39	2.59	2.44	2.48

Table 4: Nonlinear optical parameters for V_2O_5, $5ZnO/10V_2O_5$, ZnO, $10ZnO/10V_2O_5$ nanocomposites

Nanocomposites	$\bar{n}$	ϵ_o	$\chi^{(3)} \times 10^{-11}$ (esu)	$n_2 \times 10^{-11}$ (esu)
$0ZnO/10V_2O_5$	2.64	6.97	1.38	19.76
$5ZnO/10V_2O_5$	2.59	6.71	1.16	16.83
$10ZnO/0V_2O_5$	2.31	5.34	0.39	6.29
$10ZnO/10V_2O_5$	2.48	6.15	0.77	11.65

$$\varepsilon_o = \bar{n}^2, \tag{10}$$

$$\chi^{(3)} = \frac{A}{(4\pi)^4}(\bar{n}^2 - 1)^4, \tag{11}$$

$$n_2 = \frac{12\pi}{n_o}\chi^{(3)}, \tag{12}$$

where $A = 1.7 \times 10^{-10}$ esu. The numerical values of ε_o for V_2O_5, $5ZnO/10V_2O_5$ and ZnO, $10ZnO/10V_2O_5$ nanocomposites are affected by the change in the different compositions. The values of nonlinear parameters for V_2O_5, $5ZnO/10V_2O_5$ and ZnO, $10ZnO/10V_2O_5$ nanocomposites are listed in Table 4. Therefore, it can control the optical properties of these nanocomposites. Moreover, the average refractive index of ZnO is smaller than V_2O_5 and it has values in between for $5ZnO/10V_2O_5$ and $10ZnO/10V_2O_5$ nanocomposites. All these controlled properties lead us to use these nanocomposites in many applications such as photocatalytic, electronic apparatuses, and solar cells [58,59].

4 Conclusion

ZnO/V_2O_5 nanocomposites have been synthesized by the sol–gel technique. The samples are in the form of V_2O_5, $5ZnO/10V_2O_5$ and ZnO, $10ZnO/10V_2O_5$ nanocomposites. The orthorhombic structure of V_2O_5 and the hexagonal structure of ZnO were confirmed by the XRD analysis. The average crystal size of the nanocomposites of V_2O_5, $5ZnO/10V_2O_5$, and ZnO, $10ZnO/10V_2O_5$ was determined to be 25, 26, and 14.5 nm, respectively. Semi-flower, semi-sphere, and semi-tube are three different shapes that SEM captures. V_2O_5 and ZnO exhibit semi-tube forms in their pure samples. The average diameter of 0.6 m was obtained for $5ZnO/10V_2O_5$ which has a sphere-like form. However, $10ZnO/10V_2O_5$ has a semi-flower shape with several layers. Optical diffusion reflectance spectra showed the absorption edge of ZnO/V_2O_5 nanocomposites in the visible region of the spectra. The direct optical band gap showed a strong dependence on various compositions which changed in the range of 2.33–2.73 eV. On the other hand, the values of the indirect changed in the range of 2.119–2.35 eV. Our investigations have shown that ZnV_2O_6 nanostructures have the potential to be used as an energy storage material.

Acknowledgments: The authors extend their appreciation to the Deputyship for Research & Innovation, Ministry of Education in Saudi Arabia for funding this research work through the project number 445-9-750.

Funding information: This research work was funded by the Deputyship for Research & Innovation, Ministry of Education in Saudi Arabia through the project number 445-9-750.

Author contributions: All authors have accepted responsibility for the entire content of this manuscript and approved its submission.

Conflict of interest: The authors state no conflict of interest.

References

[1] Suwanboon S. Structural and optical properties of nanocrystalline ZnO powder from sol-gel method. Sci Asia. 2008;34(1):31–4.
[2] Athar T. Metal oxide nanopowder. Emerging nanotechnologies for manufacturing. USA: Elsevier; 2015. p. 343–401.
[3] Beke S. A review of the growth of V_2O_5 films from 1885 to 2010. Thin Solid Films. 2011;519(6):1761–71.
[4] Jameel MH, Saleem S, Hashim M, Roslan MS, Somaily HH, Hessin MM, et al. A comparative study on characterizations and synthesis of pure lead sulfide (PbS) and Ag-doped PbS for photovoltaic applications. Nanotechnol Rev. 2021;10(1):1484–92.
[5] Mane AA, Suryawanshi MP, Kim JH, Moholkar AV. Fast response of sprayed vanadium pentoxide (V_2O_5) nanorods towards nitrogen dioxide (NO_2) gas detection. Appl Surf Sci. 2017;403:540–50.
[6] Lao ZJ, Konstantinov K, Tournaire Y, Ng SH, Wang GX, Liu H-K. Synthesis of vanadium pentoxide powders with enhanced surface-area for electrochemical capacitors. J Power Sources. 2006;162(2):1451–4.
[7] Huo F-J, Su J, Sun Y-Q, Yin C-X, Tong H-B, Nie Z-X. A rhodamine-based dual chemosensor for the visual detection of copper and the ratiometric fluorescent detection of vanadium. Dye Pigment. 2010;86(1):50–5.
[8] Tong Z, Li N, Lv H, Tian Y, Qu H, Zhang X, et al. Annealing synthesis of coralline V_2O_5 nanorod architecture for multicolor energy-efficient electrochromic device. Sol Energy Mater Sol Cell. 2016;146:135–43.
[9] Shen K, Yang R, Wang D, Jeng M, Chaudhary S, Ho K, et al. Stable CdTe solar cell with V_2O_5 as a back contact buffer layer. Sol Energy Mater Sol Cell. 2016;144:500–8.
[10] Lee CE, Atkins RA, Gibler WN, Taylor HF. Fiber optic application for thermal switching in vanadium dioxide films. Appl Opt. 1989;28(21):4511–2.
[11] Julien C, Haro-Poniatowski E, Camacho-Lopez MA, Escobar-Alarcon L, Jímenez-Jarquín J. Growth of V_2O_5 thin films by pulsed

laser deposition and their applications in lithium microbatteries. Mater Sci Eng B. 1999;65(3):170–6.
[12] Subrahmanyam A, Reddy YBK, Nagendra CL. Nano-vanadium oxide thin films in mixed phase for microbolometer applications. J Phys D Appl Phys. 2008;41(19):195108.
[13] Gökdemir FP, Özdemir O, Kutlu K. Comparison of structural and electrochemical properties of V_2O_5 thin films prepared by organic/inorganic precursors. Electrochim Acta. 2014;121:240–4.
[14] Zargar RA, Arora M, Ahmad M, Hafiz AK. Synthesis and characterization of vanadium doped zinc oxide thick film for chemical sensor application. 2015;2015(1):196545.
[15] Saleem S, Jameel MH, Akhtar N, Nazir N, Ali A, Zaman A, et al. Modification in structural, optical, morphological, and electrical properties of zinc oxide (ZnO) nanoparticles (NPs) by metal (Ni, Co) dopants for electronic device applications. Arab J Chem. 2022;15(1):103518.
[16] Saleem S, Jameel MH, Rehman A, Tahir MB, Irshad MI, Jiang ZY, et al. Evaluation of structural, morphological, optical, and electrical properties of zinc oxide semiconductor nanoparticles with microwave plasma treatment for electronic device applications. J Mater Res Technol. 2022;19:2126–34.
[17] Maswanganye MW, Rammutla KE, Mosuang TE, Mwakikunga BW. The effect of Co and In combinational or individual doping on the structural, optical and selective sensing properties of ZnO nanoparticles. Sens Actuators B Chem. 2017;247:228–37.
[18] Rao MSR, Okada T. ZnO Nanocrystals and allied materials. Vol. 180, New Delhi: Springer; 2013.
[19] Shankar S, Saroja M, Venkatachalam M, Muthukumarasamy N, Kumar V. Influence of pH on structural and optical properties of spin coated ZnO thin films. IJIRSET. 2014;2:8990–3.
[20] Strelchuk VV, et al. Structural and optical properties of ZnO films produced by a nonvacuum chemical technique. Semiconductors. 2014;48:1145–50.
[21] Wu S, Chen Z, Wang T, Ji X. A facile approach for the fabrication of Au/ZnO-hollow-sphere-monolayer thin films and their photocatalytic properties. Appl Surf Sci. 2017;412:69–76.
[22] Purohit A, Chander S, Sharma A, Nehra SP, Dhaka MS. Impact of low temperature annealing on structural, optical, electrical and morphological properties of ZnO thin films grown by RF sputtering for photovoltaic applications. Opt Mater (Amst). 2015;49:51–8.
[23] Wang CC. Empirical relation between the linear and the third-order nonlinear optical susceptibilities. Phys Rev B. 1970;2(6):2045.
[24] Liu X, Zeng J, Yang H, Zhou K, Pan D. RSC Advances REVIEW V_2O_5–based nanomaterials: synthesis and their applications. RSC Adv. 2018;8:4014–31. doi: 10.1039/C7RA12523B.
[25] Chasta G, Suthar D, Thakur A, Kannan MD, Dhaka MS. Comprehensive investigation on influence of copper doping on physical properties of CdSe thin films for solar cell applications. Mater Res Bull. 2022;152:111845.
[26] Kumari S, Suthar D, Kannan MD, Kumari N, Dhaka MS. Understanding the grain growth mechanism in CdS thin films by $CdCl_2$ treatment and thermal annealing evolution. Opt Mater (Amst). 2022;123:111900.
[27] Taleb R, Hadeel R, Thamer SM, Abdullah A, Juzsakova T, Al N. Synthesis, characterization of V_2O_5 nanoparticles and determination of catalase mimetic activity by new colorimetric method. J Therm Anal Calorim. 2021;145(2):297–307. doi: 10.1007/s10973-020-09725-5.
[28] Boaes Mendonça LT, Bezerra AG, Mendes de Azevedo W. Preparation and characterization of V_2O_5 and V_2O_5/PANI nanocomposite by laser ablation technique in liquid. Mater Chem Phys. 2021;273:125084. doi: 10.1016/j.matchemphys.2021.125084.
[29] Ahmed NM, Sabah ZH. Characterization of V_2O_5 nanorods grown by spray pyrolysis technique. J Mater Sci Mater Electron. 2016;27(5):4613–21. doi: 10.1007/s10854-016-4338-3.
[30] Babar BM, Mohite AA, Patil VL, Pawar UT, Kadam LD, Kadam PM, et al. Sol-gel prepared vanadium oxide for photocatalytic degradation of methylene blue dye. Mater Today Proc. 2021;43:2673–7. doi: 10.1016/j.matpr.2020.04.205.
[31] Bokov D, Turki Jalil A, Chupradit S, Suksatan W, Javed Ansari M, Shewael IH, et al. Nanomaterial by sol-gel method: synthesis and application. 2021;2021(1):5102014.
[32] Rashad M, Darwish AAA. Blue shift of band gap for vanadyl 2,3-naphthalocyanine (VONc) thin films monitored at thermal effect. Mater Res Express. 2018;5(2):026402. doi: 10.1088/2053-1591/aa9ef3.
[33] Chandekar KV, Alkallas FH, Trabelsi AB, Shkir M, Hakami J, Khan A, et al. Improved linear and nonlinear optical properties of PbS thin films synthesized by spray pyrolysis technique for optoelectronics: An effect of Gd^{3+} doping concentrations. Phys B Condens Matter. 2022;641:414099.
[34] Shkir M, Chandekar KV, Khan A, Alshahrani T, El-Toni AM, Sayed MA, et al. Tailoring the structure-morphology-vibrational-optical-dielectric and electrical characteristics of Ce@ NiO NPs produced by facile combustion route for optoelectronics. Mater Sci Semicond Process. 2021;126:105647.
[35] Fabrication of ZnO-SiO_2 nanocomposite materials prepared by a spray pyrolysis for the photocatalytic activity under UV and Sunlight irradiations fabrication of ZnO-SiO_2. In:IOP Conference Series: Materials Science and Engineering; 2020. doi: 10.1088/1757-899X/778/1/012105.
[36] Faisal M, Ibrahim AA, Harraz FA, Bouzid H, Al-Assiri MS, Ismail AA. SnO_2 doped ZnO nanostructures for highly efficient photocatalyst. J Mol Catal A Chem. 2015;397:19–25.
[37] Urbach F. The long-wavelength edge of photographic sensitivity and of the electronic absorption of solids. Phys Rev. 1953;92(5):1324.
[38] Mohamed GA, El-Moiz ABA, Rashad M. Li-doping effects on the electrical properties of ZnO films prepared by the chemical-bath deposition method. Phys B Condens Matter. 2005;370(1–4):158–67.
[39] El-Menyawy EM, Elagamey AA, Elgogary SR, El-Enein RANA. Synthesis, crystal structure and thin-film-optical properties of 3-amino-2-(2-nitrophenyl) diazinyl-3-(morpholin-1-yl) acrylonitrile. Spectrochim Acta Part A Mol Biomol Spectrosc. 2013;108:75–81.
[40] Srikant V, Clarke DR. On the optical band gap of zinc oxide. J Appl Phys. 1998;83(10):5447–51.
[41] Debanath MK, Karmakar S. Study of blueshift of optical band gap in zinc oxide (ZnO) nanoparticles prepared by low-temperature wet chemical method. Mater Lett. 2013;111:116–9.
[42] Sáenz-Trevizo A, Amézaga-Madrid, Pizá-Ruiz, Antúnez-Flores W, Miki-Yoshida M. Optical band gap estimation of ZnO nanorods. Mater Res. 2016;19:33–8.
[43] Shaalan NM, Rashad M, Abdel-Rahim MA. CuO nanoparticles synthesized by microwave-assisted method for methane sensing. Opt Quantum Electron. 2016;48(12):2–12. doi: 10.1007/s11082-016-0802-9.
[44] Scanlon DO, Walsh A, Morgan BJ, Watson GW. An ab initio study of reduction of V_2O_5 through the formation of oxygen vacancies and Li intercalation. J Phys Chem C. 2008;112(26):9903–11.

[45] Kenny N, Kannewurf CR, Whitmore DH. Optical absorption coefficients of vanadium pentoxide single crystals. J Phys Chem Solids. 1966;27(8):1237–46.
[46] Luo Z, Wu Z, Xu X, Du M, Wang T, Jiang Y. Impact of substrate temperature on the microstructure, electrical and optical properties of sputtered nanoparticle V_2O_5 thin films. Vacuum. 2010;85(2):145–50.
[47] Ravindra N, Srivastava VK. Variation of refractive index with energy gap in semiconductors. Infrared Phys. 1979;19(5):603–4.
[48] Tripathy SK. Refractive indices of semiconductors from energy gaps. Opt Mater (Amst). 2015;46:240–6.
[49] Moss TS. A relationship between the refractive index and the infrared threshold of sensitivity for photoconductors. Proc Phys Soc Sect B. 1950;63(3):167.
[50] Hervé, Vandamme LKJ. General relation between refractive index and energy gap in semiconductors. Infrared Phys Technol. 1994;35(4):609–15.
[51] Reddy RR, Anjaneyulu S. Analysis of the moss and Ravindra relations. Phys Status Solidi. 1992;174(2):K91–3.
[52] V, Gupta, Ravindra NM. Comments on the moss formula. Phys Status Solidi. 1980;100(2):715–9.
[53] Kumar V, Singh JK. Model for calculating the refractive index of different materials. Indian J Pure Appl Phys. 2010;48:571–4.
[54] Ravindra NM, Auluck S, Srivastava VK. On the Penn gap in semiconductors. Phys Status Solidi. 1979;93(2):K155–60.
[55] Wemple SH, DiDomenico Jr M. Behavior of the electronic dielectric constant in covalent and ionic materials. Phys Rev B. 1971;3(4):1338.
[56] Ticha H, Tichy L. Semiempirical relation between non-linear susceptibility (refractive index), linear refractive index and optical gap and its application to amorphous chalcogenides. J Optoelectron Adv Mater. 2002;4(2):381–6.
[57] Shkir M, Khan ZR, Khan A, Chandekar KV, Sayed MA, AlFaify S. A comprehensive study on structure, opto-nonlinear and photoluminescence properties of Co_3O_4 nanostructured thin films: An effect of Gd doping concentrations. Ceram Int. 2022;48(10):14550–9.
[58] Shkir M, Khan A, Imran M, Khan MA, Zargar RA, Alshahrani T, et al. Spray pyrolysis developed Nd doped Co_3O_4 nanostructured thin films and their structural, and opto-nonlinear properties for optoelectronics applications. Opt Laser Technol. 2022;150:107959.
[59] Khan ZR, Chandekar KV, Khan A, Akhter N, Sayed MA, Shkir M, et al. An impact of novel Terbium (Tb) doping on key opto-nonlinear optical characteristics of spray pyrolyzed NiO nanostructured films for opto-nonlinear applications. Mater Sci Semicond Process. 2022;138:106260.